The Astrophysical Journal, 615:228–241, 2004 November 1

ABUNDANCES OF METAL-RICH H II REGIONS IN M51[1]

Fabio Bresolin
Institute for Astronomy, 2680 Woodlawn Drive, Honolulu, HI 96822; bresolin@ifa.hawaii.edu

and

Donald R. Garnett and Robert C. Kennicutt, Jr.
Steward Observatory, University of Arizona, 933 North Cherry Avenue, Tucson, AZ 85721; dgarnett@as.arizona.edu, robk@as.arizona.edu
Received 2004 April 26; accepted 2004 July 7

ABSTRACT

We have obtained multiobject spectroscopy of H II regions in the spiral galaxy M51 with the Keck I telescope and the Low Resolution Imaging Spectrometer. For 10 objects we have detected the auroral line [N II] λ5755, while [S III] λ6312 has been measured in seven of these. This has allowed us to measure the electron temperature of the gas and to derive oxygen, sulfur, and nitrogen abundances for the 10 H II regions. Contrary to expectations from previous photoionization models of a few H II regions in M51 and from strong-line abundance indicators, the O/H abundance is below the solar value for most objects, with the most metal-rich H II regions, P203 and CCM 72, having $\log(\mathrm{O/H}) = -3.16$ [$\sim$1.4(O/H)$_\odot$] and $\log(\mathrm{O/H}) = -3.29$ [$\sim$1.0 (O/H)$_\odot$], respectively. The reduction of O/H by factors of up to 2 or 3 with respect to previous *indirect* determinations has important consequences for the calibration of empirical abundance indicators, such as R_{23}, in the abundance and excitation range found in the central regions of spiral galaxies. The abundance gradients in these galaxies can therefore be considerably flatter than those determined by using such empirical calibrations. The H II regions with a measured electron temperature span the range (0.19–1.04) R_0 in galactocentric radius and indicate a shallow abundance gradient for M51: -0.02 ± 0.01 dex kpc^{-1}. The S/O abundance ratio is found to be similar to previous determinations of its value in other spiral galaxies, $\log(\mathrm{S/O}) \approx -1.6$. Therefore, we find no evidence for a variation in massive-star initial mass function or nucleosynthesis at high oxygen abundance. An overabundance of nitrogen is measured, with $\log(\mathrm{N/O}) \simeq -0.6$. On the basis of our new abundances, we revise the effective yield for M51, now found to be almost 4 times lower than previous estimates, and we discuss this result in the context of chemical evolution in galactic disks. Features from Wolf-Rayet stars (the blue bump at 4660 Å and the C III line at 5696 Å) are detected in a large number of H II regions in M51, with the C III λ5696 line found preferentially in the central, most metal-rich objects.

Subject headings: galaxies: abundances — galaxies: individual (NGC 5194) — galaxies: ISM — galaxies: spiral — H II regions

1. INTRODUCTION

Measuring the chemical abundances of gaseous nebulae is a crucial step to understanding the chemical evolution and the nucleosynthesis in spiral galaxies. Historically, one of the main obstacles has been the unavailability of electron temperatures (T_e) at high metallicity. This is because of the enhanced cooling via far-IR lines causing the faint auroral lines that are necessary to determine T_e (e.g., [O III] λ4363, [N II] λ5755, and [S III] λ6312) to drop below detectability in the spectra of H II regions. This difficulty affects the observations of nebulae lying in the inner portions of most spiral galaxies, where the oxygen abundance can exceed the solar value [$\log(\mathrm{O/H})_\odot = -3.31$; Allende Prieto et al. 2001]. To make this important astrophysical problem tractable, strong-line methods have been calibrated and almost universally adopted for the study of abundance gradients in spiral galaxies and, more recently, to estimate chemical abundances in high-redshift star-forming galaxies (Alloin et al. 1979; Pagel et al. 1979; Edmunds & Pagel 1984; Dopita & Evans 1986; McGaugh 1991; Díaz & Pérez-Montero 2000; Pilyugin 2000; Kewley & Dopita 2002; Denicoló et al. 2002; Kobulnicky et al. 2003; Pettini & Pagel 2004). While these methods can be calibrated empirically at low metallicity, nebular photoionization models have provided the necessary calibration at high metallicity (around the solar value and above), because of the lack of reliable H II region abundances.

From the observations of a few extragalactic H II regions that were believed to be extremely metal-rich (Kinkel & Rosa 1994; Díaz et al. 2000; Castellanos et al. 2002; Kennicutt et al. 2003), a disconcerting discrepancy emerges between T_e-based oxygen abundances and those derived through indirect means, the former being smaller by factors of a few. These results suggest that the oxygen abundance in the inner disks of spiral galaxies barely exceeds the solar value, while strong-line methods suggest abundances 2–3 times higher.

It is clear that this is exploration ground for large-aperture telescopes, given the faintness of the auroral lines that one needs to measure to obtain electron temperatures at high metallicity. A first step in this direction has been taken by Garnett et al. (2004), who used the 6.5 m MMT telescope at Mount Hopkins, Arizona, to obtain electron temperatures from the [N II] λ5755 line for two H II regions in M51, CCM 10 and CCM 72. The H II regions in this galaxy have long been considered extremely metal-rich, on the basis of their very low excitation (weak [O III] $\lambda\lambda$4959, 5007 lines relative to Hβ) and the results of photoionization models by Díaz et al. (1991).

[1] The data presented herein were obtained at the W. M. Keck Observatory, which is operated as a scientific partnership among the California Institute of Technology, the University of California, and the National Aeronautics and Space Administration. The observatory was made possible by the generous financial support of the W. M. Keck Foundation.

The metallicity obtained by Garnett et al. (2004), however, is roughly a factor of 3 smaller, barely exceeding the solar O/H value in the most metal-rich object, CCM 72.

In this paper we present an enlarged sample of H II regions in M51, observed with the Keck I telescope. The deeper spectra we obtained allowed us to measure the [N II] λ5755 line in 10 H II regions, in conjunction with [S III] λ6312 in seven of them. The larger number of objects and the measurement of two auroral lines increases our confidence in the conclusions drawn in the previous work. These observations, together with the data reduction, are described in § 2. The determination of electron temperatures and chemical abundances is presented in § 3. Major results on the oxygen, nitrogen, and sulfur abundances can be found in § 4. The impact of the resulting abundances on the calibration of strong-line methods is discussed in § 5. The Wolf-Rayet (W-R) features detected among these H II regions are briefly presented in § 6. A few considerations about effective yields and the gas fractions in M51 are addressed in § 7, and we summarize our conclusions in § 8.

2. OBSERVATIONS

Spectroscopic observations of H II regions in M51 were carried out on the night of 2003 April 24 at the W. M. Keck Observatory on Mauna Kea, using the Keck I telescope equipped with the Low Resolution Imaging Spectrometer (Oke et al. 1995). The night was photometric, with seeing at or below 1″. Using the blue and red channels of the spectrograph with a dichroic beam splitter, we obtained simultaneous observations at wavelengths below and above ~5300 Å. For the blue setting a 600 line mm^{-1} grism blazed at 4000 Å was used, providing spectra with a resolution of 4 Å FWHM on a mosaic of two 2K × 4K Marconi CCDs down to the UV atmospheric cutoff. For the red spectra the main observations, covering roughly the 5300–7200 Å wavelength range, were carried out with a 900 line mm^{-1} grating blazed at 5500 Å (3.5 Å resolution) and a 2K × 4K SITe CCD. Additional spectra with a 400 line mm^{-1} grating blazed at 8900 Å (7 Å resolution, 7000–10,000 Å approximate coverage) were obtained for the measurement of the near-IR sulfur lines at 9069 and 9532 Å. However, because of the limited near-IR extension of the calibration data, only the 9069 Å fluxes are useful, and the λ9532 fluxes were estimated from the theoretical ratio $F(9532)/F(9069) = 2.44$.

Two slit masks were used for the multiobject spectroscopy, containing 21 and 16 slits 1.″2 wide with slit lengths typically in the 10″–20″ range. The slits were oriented in the north-south direction, and the air mass during the observations was below 1.3. Archival *V*, *R*, and Hα images of M51 provided the necessary astrometry for the mask preparation. The target H II regions were selected among the brightest available in M51. A finding chart is shown in Figure 1. Five objects are in common with the previous work by Bresolin et al. (1999): CCM 10, 53, 55, 71A, and 72 (catalog numbers from Carranza et al. 1969).

The observations analyzed in this paper consist of 2 × 1800 s exposures in each of the 600/4000 and 900/5500 setups for the first mask (objects east of the galactic nucleus) and 3 × 1800 s in each setup for the second (west of the nucleus). Two 900 s exposures were used for the near-IR (400/8900) spectra. The spectrum from each slit was treated as a separate spectrum and reduced with common IRAF[2] routines. Standard-star spectra obtained at the start, middle, and end of the night provided the flux calibration. A standard extinction curve for Mauna Kea was adopted for the atmospheric extinction correction (Krisciunas et al. 1987).

The spectral region common to the red and near-IR spectra was used for flux normalization, together with the flux in the Paschen 9 and Paschen 10 lines relative to Hβ when available. This procedure introduced some additional uncertainty in the [S III] $\lambda\lambda$9069, 9532/[S III] λ6312 line flux ratio, from which the electron temperature in the intermediate-excitation zone is derived (see § 3). Given the insufficient useful overlap between the blue and red spectra, emission-line fluxes in the red spectra were adjusted relative to the fluxes in the blue spectra by scaling the flux in the Hα line so that Hα/Hβ = 3.00 as in case B at $T_e = 6000$ K. The ratio of the [N II] $\lambda\lambda$6548, 6583 to [N II] λ5755 line fluxes, from which the electron temperature in the low-excitation zone is derived, is unaffected by scaling errors, as these lines fall in the same spectra (the 900/5500 ones). Moreover, this ratio is also largely insensitive to uncertainties in reddening because of the small wavelength baseline involved.

The reddening coefficient $C(\mathrm{H}\beta)$ was determined from the Balmer decrement using the Hβ, Hγ, and Hδ lines, adopting the case B theoretical ratios at $T_e = 6000$ K and the interstellar reddening law of Cardelli et al. (1989). We have measured the [N II] λ5755 auroral line in 10 H II regions. Of these objects, [S III] λ6312 has been measured in seven cases. The IR spectrum of CCM 57A, however, fell outside the area covered by the CCD, and therefore, for this object we could not measure T[S III] in the way outlined in § 3. The [O III] λ4363 line remained undetected in all objects, while [O II] λ7325 was detected in CCM 10, 57, 71A, and 72, however, with a generally poor signal-to-noise ratio. Besides those in the two nebulae in common with the study by Garnett et al. (2004), this is the first time that auroral lines have been measured in a large number of H II regions in M51. We concentrate the rest of our analysis on the 10 objects with a measured [N II] λ5755 line, as information on electron temperatures and chemical abundances can be obtained directly only for these H II regions. The fluxes for their most important lines, corrected for reddening and normalized to $F(\mathrm{H}\beta) = 100$, are presented in Table 1, where each H II region is identified by its CCM number. The H II region P203, 7″ west and 61″ north of the M51 nucleus, which is not included in the Carranza et al. (1969) catalog, is identified from Petit et al. (1996). The errors quoted in the table reflect uncertainties in the flat-fielding and the flux calibration, as well as statistical errors, which dominate in the case of the fainter lines (e.g., the auroral lines). The comparison concerning line fluxes for objects also studied by other authors, in particular Bresolin et al. (1999) and Garnett et al. (2004; CCM 10 and CCM 72), is generally good. The agreement with these works is typically at the 5% level or better for the [N II] and [S II] lines and at the 15% level or better for the [O II], [O III], and [S III] lines. Notable exceptions are the [O III] lines of CCM 53 (46% larger than in the Bresolin et al. [1999] paper) and the [S III] $\lambda\lambda$9069, 9532 lines of CCM 71A (a factor of 2 smaller). At least for the latter H II region, a well-extended object with multiple emission peaks, differences in pointing can be responsible for the disagreement. Large differences are also found for CCM 10 when we compare with the line intensities reported by Díaz et al. (1991).

3. ELECTRON TEMPERATURES AND ABUNDANCES

As in our previous work on M101 (Kennicutt et al. 2003) and on the M51 H II regions CCM 72 and CCM 10 (Garnett

[2] IRAF is distributed by the National Optical Astronomy Observatory, which is operated by the Association of Universities for Research in Astronomy, Inc., under cooperative agreement with the National Science Foundation.

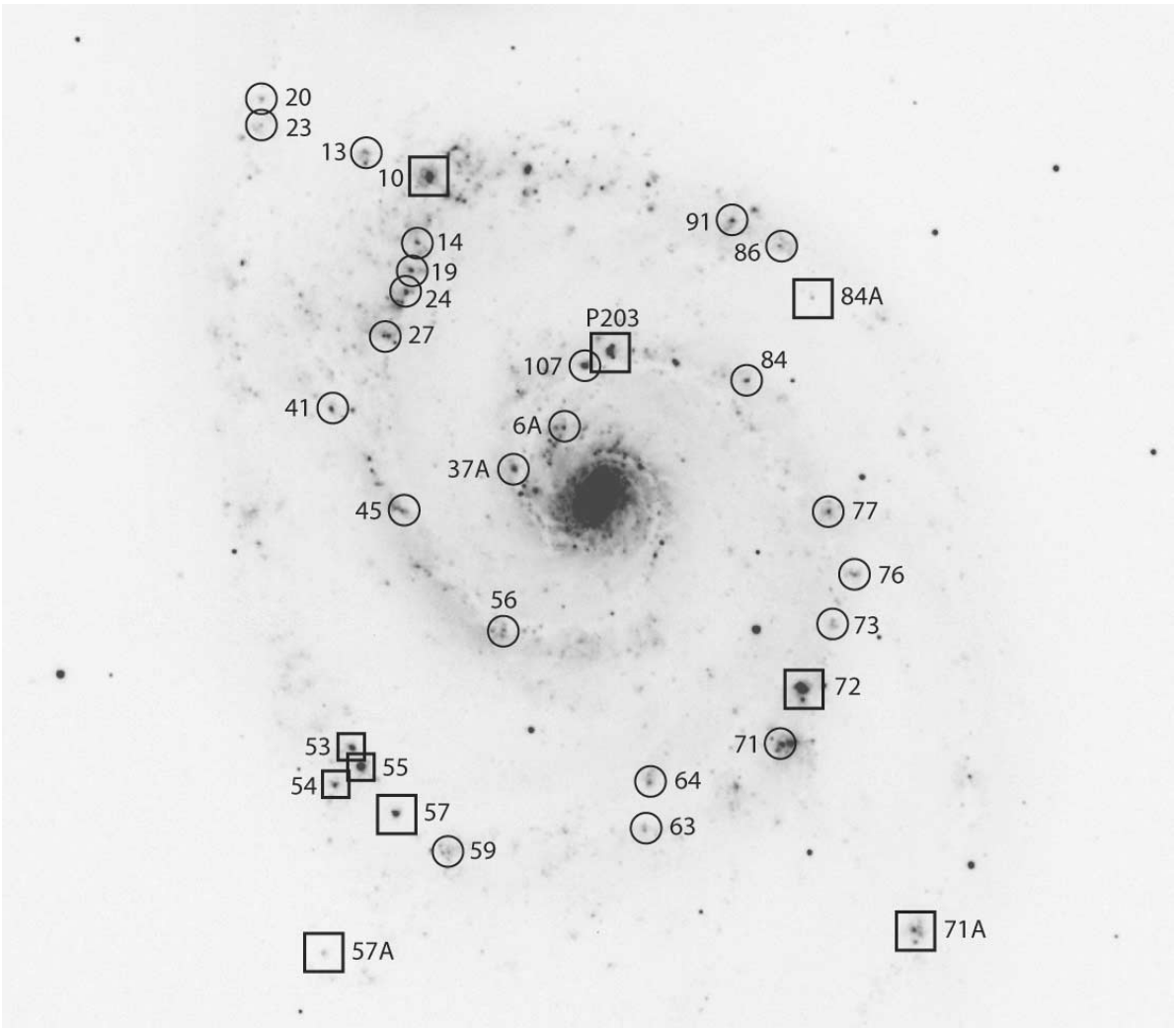

FIG. 1.—Identification of the H II regions included in the Keck multiobject observations, plotted on top of a Kitt Peak 0.9 m telescope Hα image of M51 (image courtesy of T. Rector; north is at the top, and east is to the left). Numbers are from Carranza et al. (1969), except for P203 (Petit et al. 1996). Squares mark the H II regions analyzed in this paper.

et al. 2004), we adopt a three-zone model to describe the ionization structure of an H II region. These zones are characterized by different electron temperatures T_e, each referring to different, coexisting atomic ionization stages: [O II], [N II], and [S II] in the low-ionization zone; [S III] and [Ar III] in the intermediate-ionization zone; and [O III] and [Ne III] in the high-ionization zone. The photoionization models of Garnett (1992) predict simple scaling relations between the temperatures in the different zones, applicable in a wide range of T[O III] (2000–18,000 K):

$$T[\mathrm{S\ III}] = 0.83T[\mathrm{O\ III}] + 1700\ \mathrm{K}, \quad (1)$$

$$T[\mathrm{N\ II}] = T[\mathrm{O\ II}] = 0.70T[\mathrm{O\ III}] + 3000\ \mathrm{K}. \quad (2)$$

Observational evidence in support of these relationships, in particular equation (1), has been provided by a few authors (e.g., Garnett et al. 1997; Kennicutt et al. 2003). One could consider alternative formulations, for example, the relationship between T[O II] and T[O III] given by Izotov et al. (1994), based on the grid of photoionization models by Stasinska (1990). For the same measured value of T[O II], their equation (4) would lead to T[O III] lower by a few hundred degrees relative to the Garnett (1992) equation. However, if we limit the Stasinska models to $T_{\mathrm{eff}} < 40,000$ K for the ionizing stars, as seems appropriate for the H II regions in M51, we obtain good agreement between the two different sets of photoionization models.

We established from the [S II] λ6717/[S II] λ6731 line ratio that all the H II regions are in the low-density regime ($N_e < 150$ cm^{-3}). Subsequently, using the five-level atom program *nebular* implemented in IRAF/STSDAS (Shaw & Dufour 1995), we determined the electron temperatures T[N II] (10 objects) and T[S III] (6 objects) from the emission-line ratios [N II] $\lambda\lambda$6548, 6583/[N II] λ5755 and [S III] $\lambda\lambda$9069, 9532/[S III] λ6312, respectively. The results are summarized in Table 2. As in the M101 Kennicutt et al. (2003) paper, we have updated the S III collisional strengths used by *nebular*, adopting the results by Tayal & Gupta (1999).

A good agreement is found with the independent T[N II] determinations by Garnett et al. (2004) for CCM 10 (7400^{+1000}_{-600} K) and for CCM 72 (6000 $\pm$ 300 K). To verify the H II region zone model adopted for the following analysis, we have considered the correlation between T[N II] and T[S III] for the six M51 objects for which both temperatures are available. As Figure 2 shows, the observed relation agrees very well with the

TABLE 1

Dereddened Line Fluxes and Errors

Line	CCM 10	CCM 53	CCM 54	CCM 55	CCM 57	CCM 57A	CCM 71A	CCM 72	CCM 84A	P203
[O II] λ3727	126 ± 9	129 ± 9	115 ± 8	78 ± 5	114 ± 8	104 ± 7	147 ± 10	63 ± 6	125 ± 12	32 ± 2
[Ne III] λ3869	0.7 ± 0.1	0.6 ± 0.1	1.1 ± 0.2	0.8 ± 0.1	...	12.8 ± 0.9	2.2 ± 0.2	0.4 ± 0.1	1.6 ± 0.4	...
Hδ λ4101	25 ± 2	24 ± 2	24 ± 2	23 ± 1	24 ± 2	24 ± 2	25 ± 2	25 ± 2	21 ± 2	21 ± 1
Hγ λ4340	48 ± 3	49 ± 3	46 ± 3	46 ± 3	47 ± 3	48 ± 3	46 ± 3	47 ± 3	45 ± 3	43 ± 3
He I λ4471	2.4 ± 0.2	2.9 ± 0.2	2.4 ± 0.3	2.1 ± 0.1	2.9 ± 0.2	5.6 ± 0.4	2.7 ± 0.2	2.1 ± 0.2	4.8 ± 0.5	...
[O III] λ4959	4.4 ± 0.3	11.8 ± 0.7	14.2 ± 0.9	6.7 ± 0.4	5.7 ± 0.3	60.0 ± 3.5	16.1 ± 1.0	2.4 ± 0.1	29.8 ± 1.8	1.7 ± 0.2
[O III] λ5007	12.1 ± 0.7	33.3 ± 2.0	41.5 ± 2.4	19.0 ± 1.1	15.9 ± 0.9	168.6 ± 9.9	46.1 ± 2.7	6.6 ± 0.4	84.9 ± 5.1	4.9 ± 0.3
[N II] λ5755	0.50 ± 0.04	0.54 ± 0.07	0.65 ± 0.07	0.43 ± 0.04	0.68 ± 0.09	0.48 ± 0.08	0.79 ± 0.07	0.28 ± 0.04	0.92 ± 0.15	0.15 ± 0.02
He I λ5876	7.7 ± 0.5	9.4 ± 0.6	10.0 ± 0.6	8.4 ± 0.5	10.1 ± 0.6	11.4 ± 0.7	9.3 ± 0.6	5.6 ± 0.4	13.1 ± 1.0	4.5 ± 0.3
[S III] λ6312	0.30 ± 0.03	0.31 ± 0.06	0.44 ± 0.06	0.31 ± 0.03	0.31 ± 0.07	0.62 ± 0.09	...	0.16 ± 0.03	...	...
[N II] λ6548	37 ± 3	40 ± 3	40 ± 3	38 ± 3	40 ± 3	23 ± 2	39 ± 3	33 ± 3	49 ± 4	26 ± 2
Hα λ6563	300 ± 20	300 ± 20	300 ± 20	300 ± 20	300 ± 20	300 ± 20	300 ± 20	300 ± 27	300 ± 27	300 ± 20
[N II] λ6583	112 ± 8	120 ± 8	122 ± 8	117 ± 8	124 ± 8	70 ± 5	116 ± 8	100 ± 9	144 ± 13	79 ± 5
He I λ6678	2.0 ± 0.1	2.4 ± 0.2	2.6 ± 0.2	2.1 ± 0.1	2.3 ± 0.2	3.5 ± 0.3	2.7 ± 0.2	1.8 ± 0.2	3.1 ± 0.3	1.1 ± 0.1
[S II] λ6717	27 ± 2	24 ± 2	36 ± 3	23 ± 2	26 ± 2	20 ± 1	41 ± 3	26 ± 2	19 ± 2	23 ± 2
[S II] λ6731	19 ± 1	17 ± 1	27 ± 2	18 ± 1	19 ± 1	14 ± 1	28 ± 2	20 ± 2	15 ± 1	18 ± 1
[Ar III] λ7135	2.2 ± 0.2	2.7 ± 0.3	3.6 ± 0.4	2.6 ± 0.3	2.6 ± 0.3	...	3.9 ± 0.5	1.4 ± 0.2	8.8 ± 2.8	1.7 ± 0.2
[S III] λ9069	17 ± 3	18 ± 4	17 ± 3	21 ± 4	14 ± 3	...	13 ± 3	14 ± 3	17 ± 3	9 ± 2
C(Hβ)	0.25 ± 0.05	0.10 ± 0.05	0.15 ± 0.05	0.05 ± 0.05	0.15 ± 0.05	0.05 ± 0.05	0.25 ± 0.05	0.35 ± 0.10	0.60 ± 0.10	0.21 ± 0.05
EW (Hβ) (Å)	51	92	144	74	155	300	96	61	203	47

Note.—Fluxes are given in units of H$\beta = 100$.

TABLE 2
MEASURED ELECTRON TEMPERATURES

ID	T[N II] (K)	T[S III] (K)
CCM 10	6900 ± 200	6400 ± 300
CCM 53	6900 ± 300	6400 ± 400
CCM 54	7300 ± 300	7200 ± 500
CCM 55	6600 ± 200	6100 ± 300
CCM 57	7400 ± 300	6800 ± 600
CCM 57A	7900 ± 400	...
CCM 71A	7700 ± 200	...
CCM 72	6100 ± 200	5700 ± 300
CCM 84A	7700 ± 400	...
P203	5600 ± 200	...

TABLE 3
ADOPTED ELECTRON TEMPERATURES

ID	$T(O^+, N^+, S^+)$ (K)	$T(S^{+2}, Ar^{+2})$ (K)	$T(O^{+2}, Ne^{+2})$ (K)
CCM 10	6900 ± 200	6400 ± 200	5600 ± 200
CCM 53	6900 ± 300	6400 ± 300	5600 ± 300
CCM 54	7300 ± 300	7200 ± 300	6300 ± 300
CCM 55	6600 ± 200	6100 ± 200	5200 ± 200
CCM 57	7400 ± 300	6800 ± 300	6200 ± 400
CCM 57A	7900 ± 400	7500 ± 400	7000 ± 600
CCM 71A	7700 ± 200	7300 ± 200	6800 ± 400
CCM 72	6100 ± 200	5700 ± 200	4600 ± 200
CCM 84A	7700 ± 400	7300 ± 400	6900 ± 600
P203	5600 ± 200	4800 ± 200	3700 ± 300

expectations based on the Garnett (1992) models (*dashed line*). This result is encouraging, since it supports the H II region zone model adopted here, indicating that the electron temperatures in the different excitation zones can be well established even when only one auroral line (e.g., [N II] λ5755 at low excitation) is available. We have therefore calculated the "missing" temperature for the high-ionization zone T[O III], using both equations (1) and (2) and taking a weighted average for the result when both T[N II] and T[S III] are available. This gives us electron temperature estimates for the high-, intermediate-, and low-ionization zones as described above; the results are listed in Table 3. For 6 of the 10 objects listed, we have two independent estimates of T[O III], which we have averaged, from our measured T[N II] and T[S III]. We note that the 2 σ value of T[S III] $\approx$ 5400 K for CCM 72 from Garnett et al. (2004) is very close to our result (5700 ± 300 K). The lowest temperature in our H II region sample is measured for P203, close to the galactic center, which, at $T[N\ \text{II}] = 5600$ K, is the coolest extragalactic nebula to date for which a direct electron temperature exists.

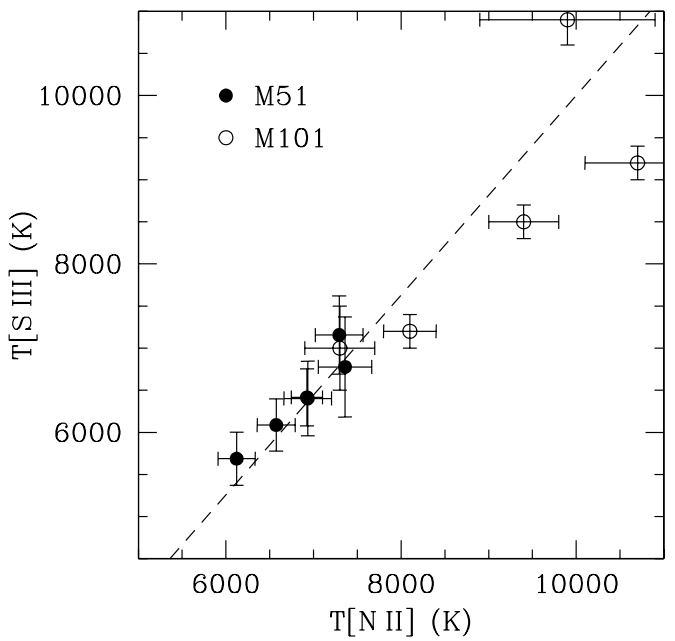

FIG. 2.—Relationship between T[N II] and T[S III] measured for H II regions in M51 (this work; *filled circles*) and M101 (Kennicutt et al. 2003; *open circles*). The model prediction from Garnett (1992) is drawn as a dashed line.

The ionic and elemental abundances derived from the electron temperatures in Table 3, using the five-level atom program, are listed in Tables 4 and 5, respectively. The associated errors derive mostly from the uncertainty in the electron temperatures. The uncertainty in the sulfur abundance is largest for CCM 57A, for which we had to rely on λ6312 alone for the S^{+2} ionic abundance because of the lack of the IR spectrum mentioned in § 2.

Ionization correction factors for sulfur are expected to be small in low-ionization nebulae, as is the case here. This is verified in Figure 3 (*top*), where the ion ratio $[(S^+ + S^{+2})/(O^+ + O^{+2})]$ is plotted against the oxygen ionization fraction O^+/O. The M51 data are in general agreement with the trend observed for H II regions in M101 (*open circles*) and NGC 2403 (*squares*), extended to higher O^+/O, even if a couple of objects (CCM 55 and 57) display a slight offset from the average relation. The dashed line in Figure 3 reproduces the sulfur ionization correction formula (Stasinska 1978; French 1981):

$$\frac{S^+ + S^{+2}}{S} = \left[1 - \left(1 - \frac{O^+}{O}\right)^{\alpha}\right]^{1/\alpha}, \qquad (3)$$

where we have used $\alpha = 2.5$ and $\log(S/O) = -1.6$, the parameters we adopted in our M101 paper. Our new observations in M51 do not justify a change in the parameters that appear in the ionization correction formula.

In the case of argon, the situation appears more complex. Unlike for sulfur, only one ionization stage (Ar^{+2}) is observed for this atomic species in the optical spectra of H II regions, and in low-ionization nebulae the amount of unseen Ar^+ can become nonnegligible. In our previous work on M101, we established that Ar^{+2}/S^{+2} is a good tracer of Ar/S, because this ratio is nearly independent of the oxygen ionization fraction (at the same time we showed that Ar^{+2}/O^{+2} is a bad tracer of Ar/O and that neon has similar problems). The plot in Figure 3 (*bottom*) suggests, however, that at high O^+/O (low ionization) Ar^{+2}/S^{+2} deviates from the roughly constant value found at higher ionization. This is likely an effect of the increase of Ar^+ with respect to Ar^{+2} at low excitation. There is, in fact, a good correlation between Ar^{+2}/S^{+2} and the hardness of the radiation field, as measured by the parameter $\eta = (O^+/O^{+2})/(S^+/S^{+2})$ (Vílchez & Pagel 1988; see Fig. 4). The ionization correction factor necessary to estimate Ar/S from Ar^{+2}/S^{+2} was obtained from the corresponding quantities in the models of Stasinska et al. (2001) and indicates that at low excitation the correction can amount to +0.2 to +0.3 dex. The shift for each H II region in

TABLE 4

Ionic Abundances

ID	O^+/H^+	O^{+2}/H^+	N^+/H^+	S^+/H^+	S^{+2}/H^+	Ne^{+2}/H^+	Ar^{+2}/H^+
CCM 10	$(3.1 \pm 0.6) \times 10^{-4}$	$(5.5 \pm 1.4) \times 10^{-5}$	$(6.8 \pm 0.7) \times 10^{-5}$	$(3.0 \pm 0.3) \times 10^{-6}$	$(7.5 \pm 1.3) \times 10^{-6}$	$(1.6 \pm 0.5) \times 10^{-5}$	$(7.2 \pm 1.5) \times 10^{-7}$
CCM 53	$(3.1 \pm 0.8) \times 10^{-4}$	$(1.5 \pm 0.6) \times 10^{-4}$	$(7.3 \pm 1.2) \times 10^{-5}$	$(2.7 \pm 0.4) \times 10^{-6}$	$(7.9 \pm 1.9) \times 10^{-6}$	$(1.5 \pm 0.7) \times 10^{-5}$	$(8.9 \pm 2.6) \times 10^{-7}$
CCM 54	$(2.1 \pm 0.5) \times 10^{-4}$	$(1.0 \pm 0.3) \times 10^{-4}$	$(6.2 \pm 0.9) \times 10^{-5}$	$(3.5 \pm 0.5) \times 10^{-6}$	$(5.6 \pm 1.1) \times 10^{-6}$	$(1.2 \pm 0.5) \times 10^{-5}$	$(8.2 \pm 2.0) \times 10^{-7}$
CCM 55	$(2.6 \pm 0.6) \times 10^{-4}$	$(1.4 \pm 0.5) \times 10^{-4}$	$(8.5 \pm 1.2) \times 10^{-5}$	$(3.3 \pm 0.4) \times 10^{-6}$	$(1.1 \pm 0.2) \times 10^{-5}$	$(3.2 \pm 1.4) \times 10^{-5}$	$(1.0 \pm 0.2) \times 10^{-6}$
CCM 57	$(2.1 \pm 0.6) \times 10^{-4}$	$(4.4 \pm 1.8) \times 10^{-5}$	$(6.1 \pm 1.0) \times 10^{-5}$	$(2.4 \pm 0.4) \times 10^{-6}$	$(5.5 \pm 1.7) \times 10^{-6}$	...	$(7.0 \pm 2.6) \times 10^{-7}$
CCM 57A	$(1.2 \pm 0.4) \times 10^{-4}$	$(2.6 \pm 1.4) \times 10^{-4}$	$(2.7 \pm 0.6) \times 10^{-5}$	$(1.5 \pm 0.3) \times 10^{-6}$	$(6.2 \pm 3.0) \times 10^{-6}$	$(8.2 \pm 5.6) \times 10^{-5}$	...
CCM 71A	$(2.0 \pm 0.4) \times 10^{-4}$	$(8.1 \pm 2.4) \times 10^{-5}$	$(4.8 \pm 0.6) \times 10^{-5}$	$(3.3 \pm 0.3) \times 10^{-6}$	$(4.1 \pm 0.5) \times 10^{-6}$	$(1.7 \pm 0.6) \times 10^{-5}$	$(8.4 \pm 1.1) \times 10^{-7}$
CCM 72	$(4.1 \pm 1.3) \times 10^{-4}$	$(1.0 \pm 0.4) \times 10^{-4}$	$(9.6 \pm 1.5) \times 10^{-5}$	$(4.8 \pm 0.7) \times 10^{-6}$	$(9.0 \pm 1.9) \times 10^{-6}$	$(3.8 \pm 2.2) \times 10^{-5}$	$(7.2 \pm 1.8) \times 10^{-7}$
CCM 84A	$(1.7 \pm 0.6) \times 10^{-4}$	$(1.6 \pm 1.0) \times 10^{-4}$	$(6.2 \pm 1.3) \times 10^{-5}$	$(1.6 \pm 0.3) \times 10^{-6}$	$(5.3 \pm 1.1) \times 10^{-6}$	$(1.3 \pm 1.0) \times 10^{-5}$	$(1.9 \pm 0.5) \times 10^{-6}$
P203	$(3.2 \pm 0.8) \times 10^{-4}$	$(3.6 \pm 2.9) \times 10^{-4}$	$(1.1 \pm 0.2) \times 10^{-4}$	$(6.0 \pm 0.8) \times 10^{-6}$	$(9.8 \pm 1.7) \times 10^{-6}$	...	$(1.8 \pm 0.4) \times 10^{-6}$

TABLE 5
TOTAL ABUNDANCES

ID (1)	R/R_0 (2)	$12 + \log(O/H)$ (3)	$\log(N/O)$ (4)	$\log(S/O)$ (5)
CCM 10	0.59	8.56 ± 0.07	-0.66 ± 0.10	-1.54 ± 0.09
CCM 53	0.51	8.66 ± 0.09	-0.63 ± 0.14	-1.63 ± 0.13
CCM 54	0.56	8.49 ± 0.08	-0.53 ± 0.12	-1.52 ± 0.10
CCM 55	0.51	8.60 ± 0.08	-0.49 ± 0.12	-1.44 ± 0.10
CCM 57	0.51	8.40 ± 0.09	-0.54 ± 0.14	-1.50 ± 0.14
CCM 57A	0.72	8.58 ± 0.14	-0.65 ± 0.17	-1.61 ± 0.24
CCM 71A	1.04	8.45 ± 0.07	-0.62 ± 0.10	-1.58 ± 0.08
CCM 72	0.51	8.71 ± 0.10	-0.63 ± 0.15	-1.56 ± 0.13
CCM 84A	0.44	8.52 ± 0.13	-0.44 ± 0.19	-1.64 ± 0.17
P203	0.19	8.84 ± 0.16	-0.46 ± 0.13	-1.61 ± 0.20

the diagram thus determined is shown by the vertical bars in Figure 3. This ionization correction scheme also shows that at high excitation (as for most of the M101 and NGC 2403 H II regions plotted) a moderate negative correction (approximately equal to -0.1 dex) should be applied to the observed Ar^{+2}/S^{+2} ratios to recover the real Ar/S ratios. This removes most of the apparently decreasing trend of Ar/S with oxygen ionization fraction suggested at first from Figure 3.

4. RESULTS FOR OXYGEN, SULFUR, AND NITROGEN

The somewhat surprising result we obtain concerns the typical oxygen abundance of the M51 H II regions studied here: for most objects O/H is below the solar value [$\log(O/H)_\odot = -3.31$; Allende Prieto et al. 2001] and reaches $\sim$1.4 times the solar value for P203 [$\log(O/H) = -3.16$], the most oxygen-rich H II region in our sample. This contrasts with the results of detailed photoionization models by Díaz et al. (1991), who

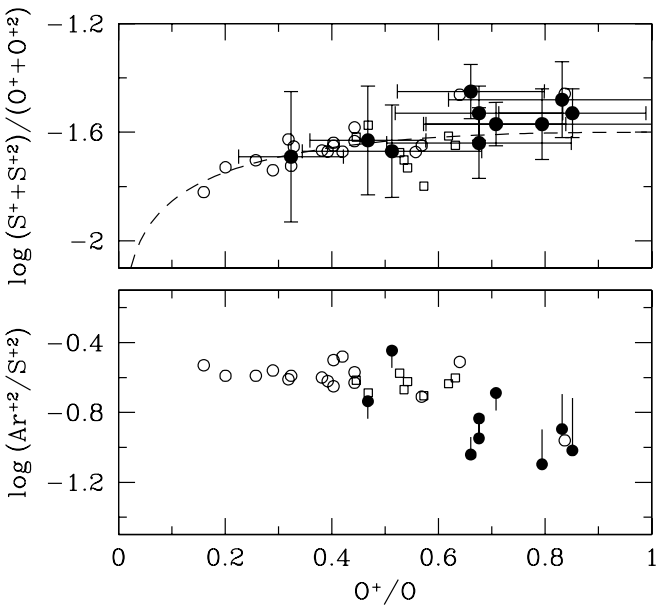

FIG. 3.—*Top*: Ion ratio $\left(S^+ + S^{+2}\right)/\left(O^+ + O^{+2}\right)$ plotted against the oxygen fractional ionization O^+/O for our sample of objects in M51 (*filled circles with error bars*) and for objects studied in M101 (Kennicutt et al. 2003; *open circles*) and in NGC 2403 (Garnett et al. 1997; *squares*). Eq. (3) for the sulfur ionization correction factor provides the dashed curve. *Bottom*: Ar^{+2}/S^{+2} plotted against O^+/O for the same sample of objects as above. A correlation with ionization seems to occur at large O^+/O values. The vertical bars show the estimated correction factors for the M51 H II regions (see text for explanation).

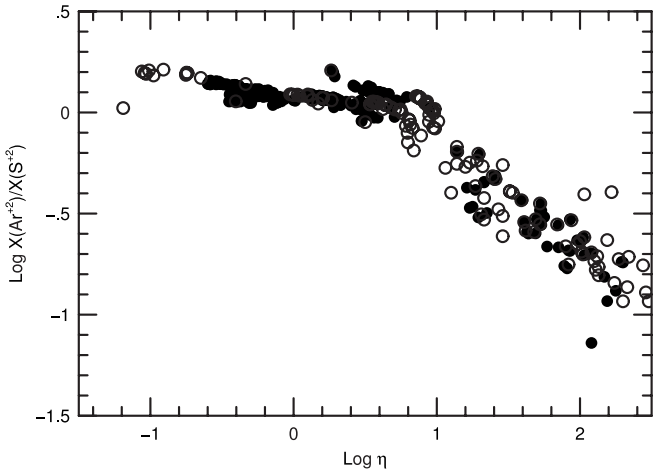

FIG. 4.—Predicted correlation between the $X(Ar^{+2})/X(S^{+2})$ ionic fraction and the radiation softness parameter η from the models of Stasinska et al. (2001). The latter are plotted for an upper limit of the initial mass function of 120 $M_\odot$ (*filled circles*) and 30 $M_\odot$ (*open circles*) for both extended and instantaneous bursts. The ionization correction factor used to obtain the abundance ratio Ar/S from Ar^{+2}/S^{+2} can be estimated from the reciprocal of $X(Ar^{+2})/X(S^{+2})$ in this plot.

estimated highly supersolar abundances between $\log(O/H) = -2.9$ and $\log(O/H) = -2.6$ for their objects (CCM 10 and CCM 72 are in common with our sample), and thus confirms the findings of Garnett et al. (2004). The concept of M51 as a very metal-rich (largely over solar) spiral galaxy, supported since the early 1990s by the above-mentioned models and the accepted calibrations of several empirical abundance determination methods, in particular R_{23} (Vila-Costas & Edmunds 1992), is not fully supported by our data. The results for P203, on the other hand, suggest that the central region of the galaxy, where the excitation is very low, contains nebulae with an O/H ratio at least 40% larger than the solar value. The discussion of additional low-excitation H II regions near the M51 nucleus is deferred to the end of § 5.

Column (2) in Table 5 lists the deprojected distance from the galaxy center in units of the isophotal radius ($R_0 = 5'.4$, corresponding to 13.2 kpc if the distance 8.4 Mpc is adopted from Feldmeier et al. [1997]). Our data span the disk from $R/R_0 = 0.19$ to 1.04, but the majority of the objects are concentrated around $R/R_0 = 0.5$. As a result, the radial trends of abundances and abundance ratios depend heavily on the H II regions at the two opposite extremes of the range, P203 (inner) and CCM 71A (outer). We plot the radial distribution of O/H, N/O, and S/O in Figure 5, which indicates a rather shallow O/H gradient in M51. The dashed line represents the linear regression to the data points:

$$12 + \log(O/H) = (8.72 \pm 0.09) - (0.28 \pm 0.14) R/R_0. \quad (4)$$

The gradient from equation (4) corresponds to $-(0.02 \pm 0.01)$ dex kpc^{-1}. The central O/H abundance ratio suggested by the regression is about solar or slightly above solar, but we cannot exclude a steepening of the relation at small galactocentric radii. Clearly, data for additional H II regions are needed to better constrain the abundance gradient in M51. There is considerable scatter at a given radial distance, amounting to $\sim$0.4 dex in O/H around $R/R_0 = 0.5$. This is not atypical, since scatter of a similar magnitude is observed in other well-studied spiral galaxies (Kennicutt et al. 2003; Garnett et al. 1997). Finally, the radial trend of both N/O and

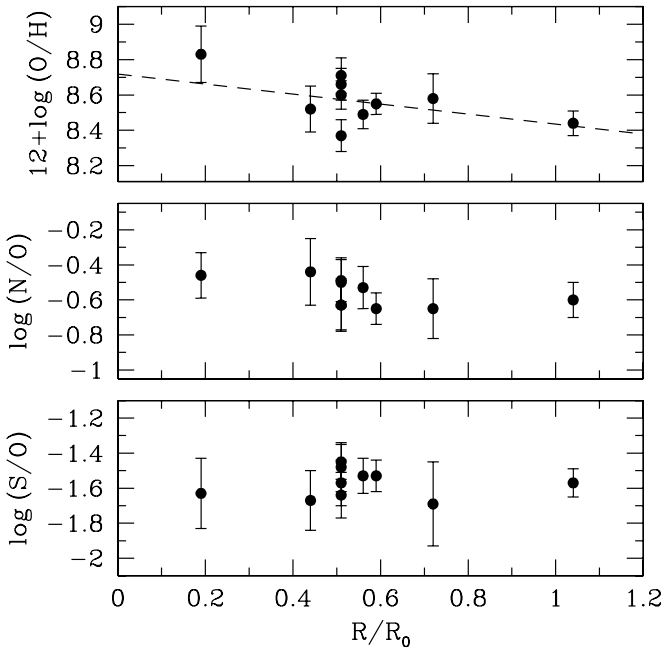

FIG. 5.—Radial trends of $12 + \log(O/H)$ (*top*), $\log(N/O)$ (*middle*), and $\log(S/O)$ (*bottom*). The dashed line represents the linear fit to the O/H radial gradient (eq. [4]).

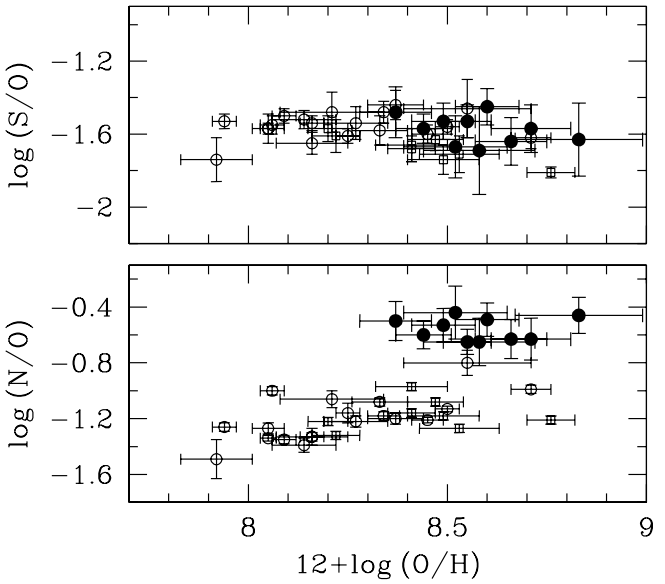

FIG. 6.—*Top*: Relationship between the S/O abundance ratio and O/H. Symbols are the same as in Fig. 3. A trend of approximately constant S/O is seen to extend beyond the solar oxygen abundance. *Bottom*: Relationship between N/O and O/H. Symbols are as in Fig. 3.

S/O is consistent with a constant value, although a very shallow N/O gradient is suggested by Figure 5.

Plots of the abundance ratios S/O and N/O as a function of O/H are shown in Figure 6. The S/O ratio (*top*) for the M51 H II regions is consistent with the approximately constant value [$\log(S/O) = -1.6$] observed in other spiral galaxies, without any evidence for a decrease as the oxygen abundance increases. The results of Díaz et al. (1991) suggested that such a decrease might occur (e.g., Garnett 2004). On the basis of our results, we therefore find no need to invoke changes in the massive-star initial mass function or in the nucleosynthesis at high metallicity (at least up to approximately the solar value).

The nitrogen abundance, shown relative to O/H in Figure 6 (*bottom*), has an average value $\log(N/O) \simeq -0.56$, higher than the value measured in H II regions of comparable oxygen abundance in galaxies such as M101 and NGC 2403. This apparent nitrogen overabundance seems consistent with the known spread of N/O at a given O/H for spiral galaxies, related to differences in star formation histories, with earlier Hubble types (M51 is classified as Sbc) having on average higher N/O ratios than later types (Henry et al. 2000; Pilyugin et al. 2003).

5. EMPIRICAL ABUNDANCE INDICATORS

The results of a quarter-century of research on nebular abundances have proved very useful for obtaining estimates of abundance gradients in spiral galaxies and of oxygen abundances of star-forming regions in the distant universe. Indirect methods (as opposed to direct methods based on the determination of electron temperatures) using ratios of strong lines have been developed by several authors; the most widely used is arguably the R_{23} empirical abundance indicator of Pagel et al. (1979). Some evidence has been mounting, however, against the accuracy of such methods in the abundance range typical of the central regions of spiral galaxies (half-solar oxygen abundance and above). This has been discussed at length in our work on M101 (Kennicutt et al. 2003), and we do not repeat the discussion here. In that paper we also presented the main issues that could complicate an analysis based on the collisionally excited lines, namely, the presence of temperature fluctuations and, at high metallicity, temperature gradients. Their effect is similar, in that the measured electron temperature is weighted toward the higher temperature zones, leading to a possible underestimate of the real nebular abundances. The reader is referred to Kennicutt et al. (2003) for further details and for a justification of the use of the collisionally excited lines. Admittedly, the issue is still open. In addition, the temperature in the [N II] zone could be overestimated by neglecting the recombination component of the 5755 Å line (see Liu et al. 2000). The lack of the line flux from [N III] at 57 μm for our M51 sample does not allow us to estimate the contribution of this recombination directly from observations. However, this contribution is likely to be small, given the small amount of N^{+2} present in low-excitation nebulae. The good agreement between the observed T[N II]–T[S III] relationship and the predicted one from Garnett (1992) also suggests that such a recombination component can be neglected to first order.

The detection of auroral lines in objects around the solar O/H ratio is prompting a revision of the abundances based on indirect methods, since relatively low abundances are found for objects that were once thought to be very metal-rich (i.e., well above the solar value: Castellanos et al. 2002; Kennicutt et al. 2003). This is also the case for the M51 H II regions analyzed in this work, and a brief assessment of a few representative empirical abundance indicators seems to be warranted at this point.

It is obvious that the abundances obtained in M51 in the present work have an important impact on most empirical calibrations. This is exemplified in Figure 7, in which we compare our direct oxygen abundances with those obtained by means of R_{23}, adopting two different calibrations: the one by Edmunds & Pagel (1984) and the one by Pilyugin (2001; see Garnett et al. [2004] for a comparison involving two other calibrations). The sample of objects shown includes, besides the M51 H II regions studied here, a number of nebulae extracted from the literature (Kennicutt et al. 2003; Garnett et al. 1997; van Zee et al. 1998;

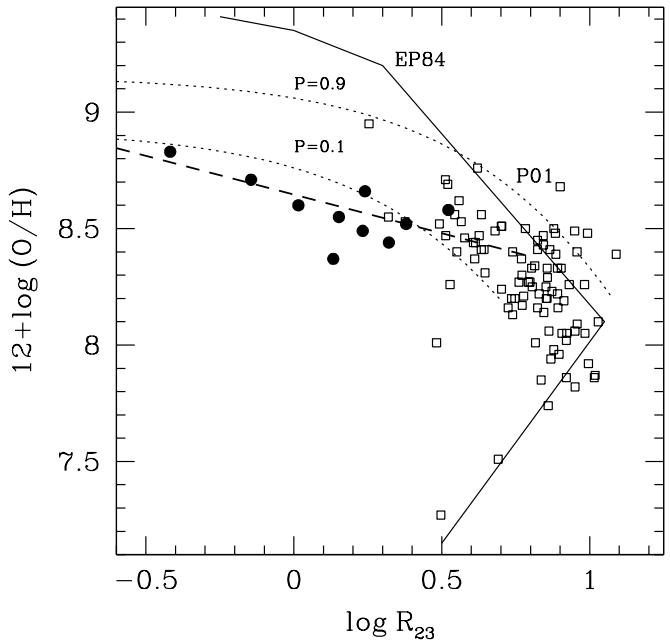

FIG. 7.—Comparison between O/H abundances obtained from measured electron temperatures (*circles*) and from the semiempirical abundance indicator R_{23} (*solid and dotted lines*). Two different R_{23} calibrations are used: Edmunds & Pagel (1984; *solid line marked EP84*) and Pilyugin (2001; *dotted lines marked P01*). Two curves are plotted for the latter, corresponding to two different values of the excitation parameter, $P = 0.1$ and 0.9. The plotted data are from the current work (*filled circles*) and from published studies of Kennicutt et al. (2003), Garnett et al. (1997), van Zee et al. (1998), Deharveng et al. (2000), Díaz & Pérez-Montero (2000), and Castellanos et al. (2002) (*squares*). The lowest excitation object, at the far left, is P203, while the most metal-rich one is CDT1 in NGC 1232 (Castellanos et al. 2002). The dashed line is a fit to the M51 points, except CCM 84A: $12 + \log(\mathrm{O/H}) = 8.64 - 0.33 \log R_{23}$.

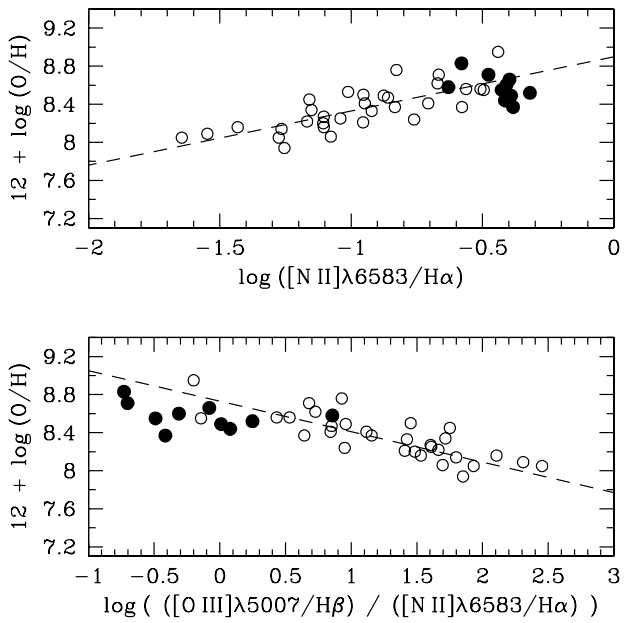

FIG. 8.—*Top*: O/H abundances obtained with the direct method plotted against the line ratio [N II] λ6583/Hα. Data are from this work (*filled circles*) and from Kennicutt et al. (2003), Garnett et al. (1997), and Castellanos et al. (2002) (*open circles*). The dashed line is the regression taken from Pettini & Pagel (2004), obtained from a fit to a larger sample of H II regions. *Bottom*: Same as above, for the ([O III] λ5007/Hβ)/([N II] λ6583/Hα) index.

Deharveng et al. 2000; Díaz & Pérez-Montero 2000; Díaz et al. 2000; Castellanos et al. 2002). We note that for the high-metallicity object CDT1 in NGC 1232 studied by Castellanos et al. (2002) we derive, using their line fluxes, an O/H value smaller by 0.13 dex than their published abundance, $12 + \log(\mathrm{O/H}) = 8.95$. Our results on the M51 H II regions clearly demonstrate the failure of the existing R_{23} calibrations at low excitation ($\log R_{23} < 0.5$), since they overestimate the abundances by 50%–400%. This discrepancy corresponds to electron temperatures smaller by approximately 10%–15% compared with our measured values (about 3–4 σ). For CCM 72 and CCM 10, the [O II] temperatures modeled by Díaz et al. (1991; 4800 and 6000 K, respectively) lie 4 and 6 σ below our measurements, respectively.

This result has fundamental consequences for the studies of abundance gradients in spiral galaxies based on this empirical indicator (e.g., Zaritsky et al. 1994; Vila-Costas & Edmunds 1992), and the actual gradients in the central regions are in general much flatter than those reported in these works. The discrepancy is also not peculiar to R_{23}. As an example, Pettini & Pagel (2004) have considered an empirical abundance calibration of two line indices involving the nitrogen lines [N II] λ6583/Hα (see also Denicoló et al. 2002) and ([O III] λ5007/Hβ)/([N II] λ6583/Hα). We show in Figure 8 the position occupied in the corresponding diagrams by the M51 H II regions. A decrease in the slope at low excitation is noted with respect to the Pettini & Pagel (2004) calibrations (*dashed lines*), indicating a flattening around $12 + \log(\mathrm{O/H}) = 8.6$, which, however, also reflects the large nitrogen abundance found in M51 from our analysis. Figure 9 shows instead how the O/H abundances derived through the P-method (Pilyugin 2001) compare with direct abundances. In this plot, only objects that the P-method predicts have $12 + \log(\mathrm{O/H}) > 8.2$ (the quoted range of validity for this method in the high-abundance regime) are plotted. This indicator seems to be afflicted by severe difficulties in a wide abundance range. The general conclusion we can draw is that great caution is necessary when using strong-line empirical abundance indicators for low-excitation H II regions. Erroneous results can be obtained in the inner disks of spiral galaxies up to a factor of a few.

How low can the excitation in M51 H II regions be? We report in Table 6 the line fluxes, normalized to H$\beta = 100$, measured for the H II regions besides P203 belonging to the central zone of the galaxy [$R = (0.12$–$0.36)R_0$]. No auroral line was

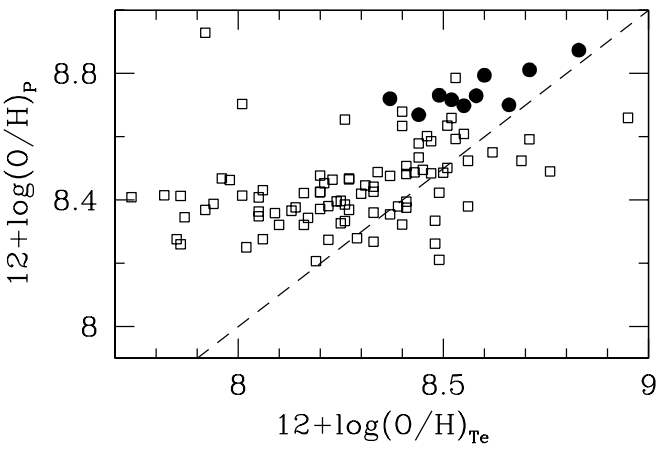

FIG. 9.—Comparison of direct O/H abundances and those obtained through the P-method of Pilyugin (2001). The data are from the current work (*filled circles*) and from Kennicutt et al. (2003), Garnett et al. (1997), van Zee et al. (1998), Deharveng et al. (2000), Díaz & Pérez-Montero (2000), and Castellanos et al. (2002) (*squares*). Only objects that the P-method predicts have $12 + \log(\mathrm{O/H}) > 8.2$ are plotted.

TABLE 6

LINE FLUXES OF LOW-EXCITATION OBJECTS

ID	R/R_0	$C(\mathrm{H}\beta)$	EW($\mathrm{H}\beta$) (Å)	[O II] λ3727	[O III] $\lambda\lambda$4959+5007	He I λ5876	[N II] $\lambda\lambda$6548+6584	[S II] $\lambda\lambda$6717+6731	T[N II] (Upper Limit) (K)	$12 + \log(\mathrm{O}/\mathrm{H})$ (Lower Limit)
CCM 6A	0.12	0.10	55	17 ± 1	4.4 ± 0.3	3.9 ± 0.3	80 ± 4	26 ± 1	5800	8.40
CCM 37A	0.16	0.09	12	17 ± 1	4.8 ± 0.4	3.0 ± 0.3	54 ± 3	20 ± 1	6200	8.20
CCM 45	0.36	0.17	54	34 ± 2	4.2 ± 0.4	5.5 ± 0.5	116 ± 6	50 ± 3	5900	8.52
CCM 56	0.22	0.23	50	28 ± 2	8.5 ± 0.9	4.5 ± 0.5	121 ± 7	50 ± 3	5900	8.58
CCM 107	0.19	0.53	48	20 ± 1	2.6 ± 0.2	5.2 ± 0.3	98 ± 5	30 ± 2	5300	8.86

NOTE.—Fluxes are given in units of $\mathrm{H}\beta = 100$.

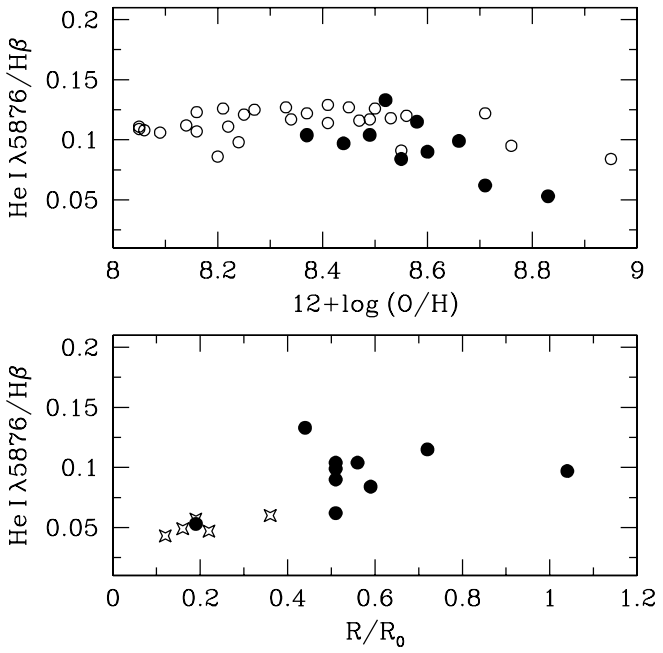

FIG. 10.—*Top*: Suggestion of a trend of decreasing He I λ5876/Hβ line ratio with abundance above $12 + \log(O/H) \approx 8.5$. The 5876 Å line has been corrected for an underlying absorption equivalent width of 0.8 Å. Objects plotted are from M51 (*filled circles*) and M101 (*open circles*). *Bottom*: Variation of He I λ5876/Hβ with galactocentric distance for M51 H II regions. The filled circles represent objects with a direct abundance determination; the open stars represent objects of low excitation found in the central region of the galaxy.

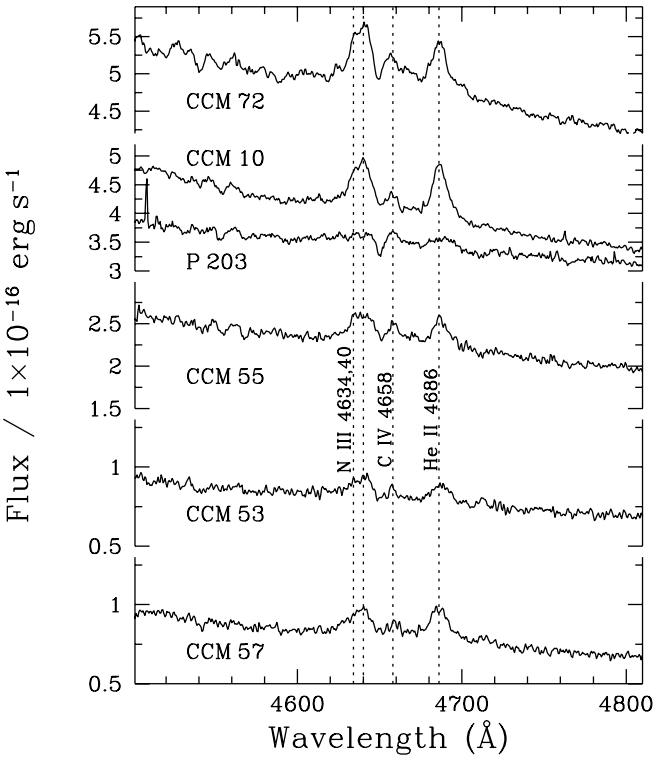

FIG. 11.—W-R stellar lines around 4660 Å detected in these six H II regions out of the 10 analyzed. The vertical dotted lines identify features.

detected in these objects; therefore, a direct abundance determination was not permited. The total [O III] $\lambda\lambda$4959, 5007 flux is just a few percent of the Hβ line flux, and the corresponding value of R_{23} is in the range -0.42 to -0.67. Because of the rather flat relationship between O/H and R_{23} at the low excitation suggested by the M51 points in Figure 7, these very low R_{23} values might still correspond to metallicities not much higher than solar ($12 + \log(O/H) \approx 8.8$–$8.9$]; however, any extrapolation to determine an oxygen abundance is at present still very uncertain. The dashed line in Figure 7 shows such an extrapolation, determined from the M51 H II regions. The highest oxygen abundance in our sample, corresponding to $\log R_{23} = -0.66$ (the value for CCM 6A, CCM 37A, and CCM 107 within ± 0.01), would be $12 + \log(O/H) \approx 8.86$ (1.5 times the solar O/H), comparable to our measured oxygen abundance for P203.

We have estimated upper limits for the [N II] electron temperature and the corresponding lower limits for the oxygen abundance from the nondetection of the [N II] λ5755 line in the spectra of the central objects. The results, summarized in Table 6, are not very compelling, and they are still consistent with abundances in the central region of M51 around the value found for P203.

Finally, we point out that the He I λ5876/Hβ line ratio correlates with both O/H (for the objects in Table 1) and galactocentric distance (objects in Tables 1 and 6), as shown in Figure 10. Together with the reduced excitation measured from the [O III]/Hβ ratio mentioned above, Figure 10 shows how the ionizing field becomes softer toward higher metallicities, above a certain abundance threshold [the He I λ5876/Hβ ratio decreases below its saturation level, at which He is completely singly ionized, for $12 + \log(O/H) \geq 8.5$; *top*] and toward the galactic central regions (*bottom*). The observed increase of the neutral helium fraction toward the metal-rich central region of M51 can be viewed as the result of the decrease in the equivalent effective temperature of the ionizing radiation field with increasing metallicity (see also Bresolin & Kennicutt 2002).

6. WOLF-RAYET STARS

The main spectroscopic signature of W-R stars (the blue bump at 4660 Å) has been detected in six of the H II regions examined in this work. As shown in Figure 11, we can clearly distinguish the stellar N III $\lambda\lambda$4634, 4641 and He II λ4686 lines in all cases, together with C IV λ4658. Given the absence of N V $\lambda\lambda$4603, 4620, the morphology of the blue bump is characteristic of late W-R subtypes (WNL). In addition, the C III λ5696 line from WC-subtype stars has been clearly detected in the two most metal-rich H II regions, CCM 72 and P203. W-R features have been detected in other M51 H II regions not analyzed in this paper. In CCM 13, 24, 41, 84A, and 91, only the blue bump is present in our spectra. Both the 4660 and 5696 Å features are seen in CCM 37A, 84, and 107, while only the 5696 Å line is visible in CCM 6A and 71 (also with 5810 Å). A marginal detection of He II λ4686 has been made in a few additional objects, as well. Note that all the nebulae (except CCM 71) for which the C III λ5696 line has been detected are located at small galactocentric radii or have large O/H abundances (CCM 72). This agrees with the known trend of increasing fraction of WC relative to WN stars with abundance (Massey 2003).

The number of WNL stars can be estimated from the total He II λ4686 line luminosity, assuming a fixed stellar luminosity of 1.6×10^{36} ergs s^{-1} (Schaerer & Vacca 1998). At the adopted distance to M51 of 8.4 Mpc, the two objects with the highest He II luminosity (CCM 10 and CCM 72) are then found to contain five or six WNL stars each. The luminosity of the remaining objects is consistent with the presence of just one or two WNL stars. These numbers are not particularly remarkable

when compared, for example, with the very large population of W-R stars discovered by Crowther et al. (2004) in H II regions of another supposedly metal-rich galaxy, M83. Reporting the detection of W-R features in solar-like abundance environments, however, is still of considerable interest, because of the trends one can establish between W-R star population properties (e.g., their subtype distribution) and metallicity. It is also relevant to point out that W-R features are found in very cool nebulae, such as the metal-rich CCM 72 and P203, supporting the idea that the presence of these evolved massive stars does not significantly affect the ionizing properties of the embedded star clusters (Bresolin & Kennicutt 2002).

7. GAS FRACTIONS, EFFECTIVE YIELDS, AND CHEMICAL EVOLUTION

A comparison of observed abundances and gas fractions in galaxies provides interesting information on the effect of gas flows on galaxy evolution. Variations of the effective yield, defined as

$$y_{\rm eff} = \frac{Z}{\ln \mu^{-1}}, \tag{5}$$

where Z is the metallicity and μ is the gas mass fraction, are sensitive to gas inflow and outflow (Edmunds 1990; Köppen & Edmunds 1999). Garnett (2002) compared effective yields, derived from global abundance, stellar mass, and gas mass properties, in a sample of 50 nearby spiral and irregular galaxies and found that $y_{\rm eff}$ varies systematically with galaxy rotation speed (and thus presumably total mass). The adopted interpretation was that the low-mass irregular galaxies, with smaller effective yields than those derived for massive spiral galaxies, were losing a large fraction of their metals to the intergalactic medium.

On the basis of our new abundances for M51, we can reevaluate its effective yield. Garnett (2002) used the measured abundance at 1 effective disk radius as a measure of the average metallicity of a spiral disk. From his Table 4, the adopted average $12 + \log({\rm O/H})$ was 9.12 for M51. Our new value for $12 + \log({\rm O/H})$ at $R_{\rm eff} = 0.6R_0$ is 8.55, a factor of 3.7 smaller. Thus, the new value of $y_{\rm eff}$ we derive is smaller by the same amount. Garnett (2002) derived $y_{\rm eff} = 0.012$ for M51, so we would obtain $y_{\rm eff} = 0.0032$ from our new data. This lower value is comparable to the values derived for smaller irregular galaxies such as IC 10 and NGC 6822 in Garnett's sample. Note also that this value of $y_{\rm eff}$ is much closer to that expected from stellar nucleosynthesis and to the value obtained from estimates of the mean metallicity and gas fraction in the solar neighborhood. If other spiral galaxies show similar reductions in $y_{\rm eff}$ when more temperature-based abundance measurements become available, it may be necessary to reexamine the conclusions of Garnett (2002) regarding which galaxies may experience significant loss of metals.

It is also interesting and important to look at the variation of $y_{\rm eff}$ across a disk galaxy to see whether gas flows play a role in the chemical evolution within the disk. A comparison between gas fraction and abundance across the disk has been made for only a few spiral galaxies to date.

We obtained the radial distribution of gas surface densities in M51 from the single-dish CO mapping of Kuno et al. (1995), measured with a 16″ beam, and from the H I 21 cm map of Tilanus & Allen (1991). Young et al. (1995) also measured the radial distribution of CO, but their much larger beam size means that the mass surface density is averaged over a much larger area. We choose not to use measurements based on interferometers (e.g., Aalto et al. 1999), as they can miss significant amounts of extended emission because they miss short antenna baselines; we note that the measurements of Aalto et al. (1999) show a very sharply peaked CO flux distribution, in rough agreement with Kuno et al. (1995). The derived molecular gas surface densities depend critically on the conversion from CO intensity to H_2 column density. We derived molecular surface densities under two assumptions for the $I({\rm CO}) - N(H_2)$ conversion factor: (1) the "standard" factor 3.0×10^{20} cm^{-2} (K km s^{-1})$^{-1}$ (Wilson 1995; which includes a contribution for helium) and (2) the smaller factor 1.3×10^{20} cm^{-2} (K km s^{-1})$^{-1}$ used by Kuno et al. (1995; adjusted here to include helium). Whichever value is used, the mass of molecular gas in M51 is quite large, and the mass surface density of H_2 exceeds that of atomic gas over much of the disk. The CO measurements do not go beyond 180″ from the nucleus, so we have smoothly extrapolated the H_2 surface densities to larger radii on the basis of an approximate exponential fit to the inner disk profile. Gas surface density distributions for a subset of our assumptions are shown in Figure 12.

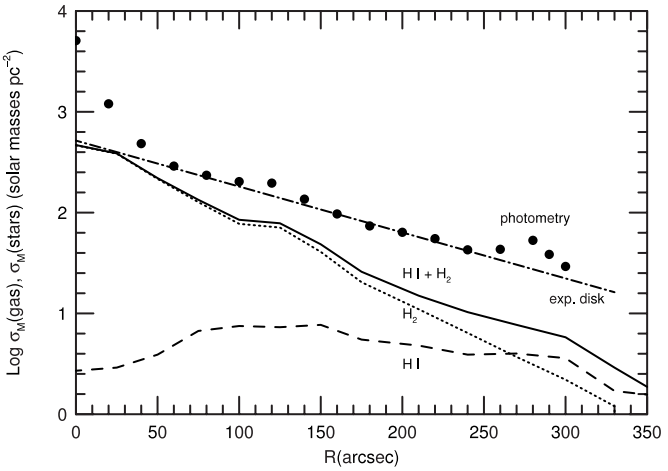

FIG. 12.—Gas and stellar mass surface density distributions in M51. The dashed line shows the H I surface density (adjusted for the presence of helium) from the data of Tilanus & Allen (1991). The dotted line shows the molecular gas profile obtained from the CO measurements of Kuno et al. (1995), assuming an $I({\rm CO}) - N(H_2)$ conversion factor of 3×10^{20} cm^{-2} (K km s^{-1})$^{-1}$. The dot-dashed line shows the mass profile for the stellar exponential disk determined as discussed in the text. The filled circles show stellar mass densities derived directly from the surface brightness data of Kuchinski et al. (2000).

The mass surface density for stars in M51 was derived from the *BVRI* surface photometry of Kuchinski et al. (2000). We converted the *I*-band surface brightnesses to mass surface densities by estimating the mass-to-light ratio (M/L) from the relations between M/L and color derived from stellar population models in Bell & de Jong (2001). From the Kuchinski et al. surface brightnesses, we estimated a central *I*-band disk surface brightness of 19.05 mag arcsec^{-2} and a disk scale length of 114″; we adopted a linear color profile with radius ranging from $B - R = 1.2$ at the center to 0.9 at 300″. The resulting stellar mass profile for the disk in M51 is shown in Figure 12 as the dot-dashed line, while the mass densities estimated directly from the photometry are shown as the circles. Note that the photometry shows evidence for a central spheroidal component.

Inspection of Figure 12 shows one curious feature: the gas surface density profile is steeper than the stellar disk profile.

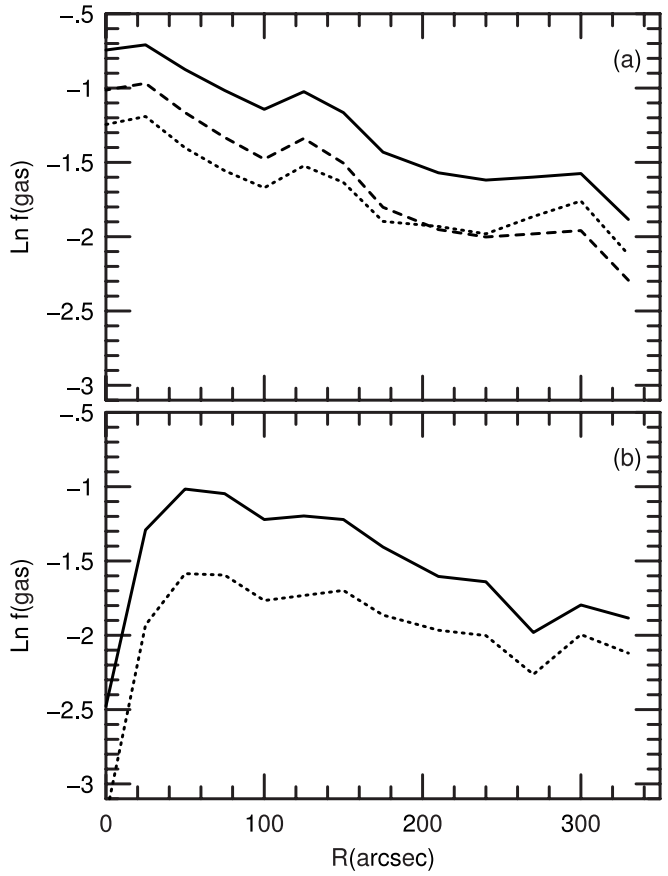

FIG. 13.—(*a*) Radial variation of the gas mass fraction for three different assumptions: molecular gas masses estimated using an $I(\mathrm{CO}) - N(\mathrm{H_2})$ conversion of 3.0×10^{20} (*solid line*), molecular gas mass densities estimated using an $I(\mathrm{CO}) - N(\mathrm{H_2})$ conversion of 1.3×10^{20} (*dashed line*), and the same gas densities as for the solid line but with stellar surface brightnesses adjusted for extinction $A(I) = 0.5$ mag (*dotted line*). (*b*) Radial variation of the gas fraction, in which the stellar mass densities were derived directly from the *I*-band photometry rather than from the underlying exponential disk. The solid line shows molecular gas densities obtained using $I(\mathrm{CO}) - (\mathrm{H_2}) = 3.0 \times 10^{20}$; the dotted line shows molecular gas densities obtained using $I(\mathrm{CO}) - N(\mathrm{H_2}) = 1.3 \times 10^{20}$.

This implies that the gas fraction decreases radially outward. We illustrate this in Figure 13*a*, which shows the radial variation in three different cases: (1) $I(\mathrm{CO}) - N(\mathrm{H_2}) = 3.0 \times 10^{20}$ (*solid line*), (2) $I(\mathrm{CO}) - N(\mathrm{H_2}) = 1.3 \times 10^{20}$ (*dashed line*), and (3) a case similar to (1) but in which the stellar surface brightnesses have been adjusted upward for an extinction of $A(I) = 0.5$ mag (*dotted curve*). In all three cases, the derived gas fraction declines by a factor of 3–4 radially outward. This behavior contrasts strongly with that seen in other spiral galaxies, for which the gas fraction increases outward (M81: Garnett & Shields 1987; NGC 4254: Henry et al. 1994; NGC 2403 and M33: Garnett et al. 1997).

We have also looked at what happens if we simply use the observed surface brightness profile rather than an underlying exponential disk to derive the stellar mass densities. The resulting gas profiles for our two assumptions of the $I(\mathrm{CO}) - N(\mathrm{H_2})$ conversion are shown in Figure 13*b*. While the resulting gas fractions for the inner disk are certainly smaller, because of the high central surface brightness, we still see a declining gas fraction with radius for $R > 50''$.

We note that a radial variation of a factor of 3 in the $I(\mathrm{CO}) - N(\mathrm{H_2})$ conversion is not sufficient to mitigate the decline in gas fraction. A factor-of-6 change in the conversion factor would be needed to flatten the gas fraction profile; such a variation is not at all predicted, even by the most extreme estimates of metallicity variation in the conversion factor (Israel 1997). A radial decline of about 1.5 mag in $A(I)$ from the center to the outer disk would also be enough to flatten the gas fraction profile. Scoville et al. (2001) found a rough radial variation in $A(V)$ for H II regions in the disk of M51, from $A(V) \approx 4$ in the inner disk to $A(V) \approx 2$ at $R = 300''$; however, it is not clear how to relate the extinction for H II regions, which are associated with gas and dust, to the extinction for the stellar disk. We also note that $A(I) = 0.5$ corresponds to $E(B - V) = 0.3$; with an observed $B-V$ of 0.6, such a correction for reddening would make M51 a very blue galaxy unless the reddening is very gray.

A radially decreasing gas fraction combined with a radially decreasing metallicity implies an effective yield that increases with metallicity. Such a variation was inferred by Vila-Costas & Edmunds (1992), but with older abundance data derived mainly from strong emission line calibrations. On the other hand, galaxies with abundances based on electron temperatures show little evidence for variations in effective yields (Garnett et al. 1997).

The peculiar gas fraction profile in M51 may also point to dynamical influences. M51 is an interacting system. Flyby interactions of this type can lead to bar formation, which induces radial flows of gas toward the center of the galaxy. Pierce (1986), Kohno et al. (1996), and Aalto et al. (1999) have presented photometric and kinematic evidence for a bar in the central regions of NGC 5194, while infrared imaging reveals that NGC 5195 has an obvious bar (e.g., the *I*-band images of Kuchinski et al. 2000). It is possible that the interaction and bar have driven gas into the central regions of M51, leading to the very steep gas profile we see. This would complicate the interpretation of the chemical evolution of this system and require dynamical and photometric modeling that is beyond the scope of this work.

8. CONCLUSIONS

We have analyzed a sample of 10 H II regions in the spiral galaxy M51 where at least one of the auroral lines [N II] λ5755 and [S III] λ6312 could be measured, and we discussed the resulting oxygen, sulfur, and nitrogen abundances. The single most remarkable result obtained is that in M51 the direct O/H abundances are considerably below the value obtained either from photoionization models (Díaz et al. 1991) or from empirical abundance indicators. So far, the calibration of the latter in the low-excitation range defined mostly by H II regions in M51 has depended on the abundances obtained from the models; therefore, the two are not independent. We have not attempted to generate improved nebular models, for example, by including more recent stellar atmospheres for the treatment of stellar ionizing fluxes. This aspect needs to be explored in the future.

The result concerning O/H has important implications for the calibration of empirical abundance indicators and in general for the determination of abundance gradients in spiral galaxies. Our result, combined with previous ones obtained for smaller samples of metal-rich H II regions by Castellanos et al. (2002), Díaz et al. (2000), and Kennicutt et al. (2003), points to shallower gradients. H II regions once believed to have O/H abundances equal to 2–3 times solar are now rarely found by the direct method to exceed the solar value, and if so by a moderate amount, up to 50%.

Our analysis has also established that in our M51 sample the abundance ratio S/O is similar to the value found at lower O/H

abundances in other spiral galaxies. We find no evidence for a decrease in S/O with increasing O/H, which would occur for a differing initial mass function and/or nucleosynthesis for massive stars. The nitrogen abundance has the mean value $\log(N/O) \simeq -0.6$, larger than in later spiral galaxies such as M101, but this can still be interpreted by using the known spread of N/O at a given oxygen abundance.

The lower oxygen abundance that we measure in M51 with respect to previous determinations has also allowed us to revise the effective yield of this galaxy. From a rather peculiar gas fraction radial profile we infer an effective yield that increases with metallicity.

The number of galaxies with reliable *direct* measurements of nebular chemical abundances extending over their whole disks, including the metal-rich central zones, is still very limited. These measurements are necessary for the correct determination of the chemical compositions in galactic disks and their interpretation in terms of chemical evolution models. The current work on M51 demonstrates that large samples of metal-rich H II regions can be efficiently studied in spiral galaxies with currently available telescopes and instrumentation.

We thank T. Rector for the Kitt Peak 0.9 m Hα image of M51 used for Figure 1. R. C. K. acknowledges NSF grant AST 03-07386 and NASA grant NAG5-8426. D. R. G. acknowledges NSF grant AST 02-03905 and NASA grant NAG5-7734.

REFERENCES

Aalto, S., Hüttemeister, S., Scoville, N. Z., & Thaddeus, P. 1999, ApJ, 522, 165
Allende Prieto, C., Lambert, D. L., & Asplund, M. 2001, ApJ, 556, L63
Alloin, D., Collin-Soufrin, S., Joly, M., & Vigroux, L. 1979, A&A, 78, 200
Bell, E. F., & de Jong, R. S. 2001, ApJ, 550, 212
Bresolin, F., & Kennicutt, R. C., Jr. 2002, ApJ, 572, 838
Bresolin, F., Kennicutt, R. C., Jr., & Garnett, D. R. 1999, ApJ, 510, 104
Cardelli, J. A., Clayton, G. C., & Mathis, J. S. 1989, ApJ, 345, 245
Carranza, G., Crillon, R., & Monnet, G. 1969, A&A, 1, 479
Castellanos, M., Díaz, A. I., & Terlevich, E. 2002, MNRAS, 329, 315
Crowther, P. A., Hadfield, L. J., Schild, H., & Schmutz, W. 2004, A&A, 419, L17
Deharveng, L., Peña, M., Caplan, J., & Costero, R. 2000, MNRAS, 311, 329
Denicoló, G., Terlevich, R., & Terlevich, E. 2002, MNRAS, 330, 69
Díaz, A. I., Castellanos, M., Terlevich, E., & García-Vargas, M. L. 2000, MNRAS, 318, 462
Díaz, A. I., & Pérez-Montero, E. 2000, MNRAS, 312, 130
Díaz, A. I., Terlevich, E., Vílchez, J. M., Pagel, B. E. J., & Edmunds, M. G. 1991, MNRAS, 253, 245
Dopita, M. A., & Evans, I. N. 1986, ApJ, 307, 431
Edmunds, M. G. 1990, MNRAS, 246, 678
Edmunds, M. G., & Pagel, B. E. J. 1984, MNRAS, 211, 507
Feldmeier, J. J., Ciardullo, R., & Jacoby, G. H. 1997, ApJ, 479, 231
French, H. B. 1981, ApJ, 248, 468
Garnett, D. R. 1992, AJ, 103, 1330
———. 2002, ApJ, 581, 1019
———. 2004, in Cosmochemistry: The Melting Pot of the Elements, ed. C. Esteban, R. J. Garcia Lopez, A. Herrero, & F. Sanchez (Cambridge: Cambridge Univ. Press), 171
Garnett, D. R., Kennicutt, R. C., Jr., & Bresolin, F. 2004, ApJ, 607, L21
Garnett, D. R., & Shields, G. A. 1987, ApJ, 317, 82
Garnett, D. R., Shields, G. A., Skillman, E. D., Sagan, S. P., & Dufour, R. J. 1997, ApJ, 489, 63
Henry, R. B. C., Edmunds, M. G., & Köppen, J. 2000, ApJ, 541, 660
Henry, R. B. C., Pagel, B. E. J., & Chincarini, G. 1994, MNRAS, 266, 421
Israel, F. P. 1997, A&A, 328, 471
Izotov, Y. I., Thuan, T. X., & Lipoyetsky, V. A. 1994, ApJ, 435, 647
Kennicutt, R. C., Jr., Bresolin, F., & Garnett, D. R. 2003, ApJ, 591, 801
Kewley, L. J., & Dopita, M. A. 2002, ApJS, 142, 35
Kinkel, U., & Rosa, M. R. 1994, A&A, 282, L37
Kobulnicky, H. A., Henry, A., & Phillips, A. C. 2003, ApJ, 599, 1031
Kohno, K., Kawabe, R., Tosaki, T., & Okamura, S. K. 1996, ApJ, 461, L29
Köppen, J., & Edmunds, M. G. 1999, MNRAS, 306, 317
Krisciunas, K., et al. 1987, PASP, 99, 887
Kuchinski, L. E., et al. 2000, ApJS, 131, 441
Kuno, N., Nakai, N., Handa, T., & Sofue, Y. 1995, PASJ, 47, 745
Liu, X.-W., Storey, P. J., Barlow, M. J., Danziger, I. J., Cohen, M., & Bryce, M. 2000, MNRAS, 312, 585
Massey, P. 2003, ARA&A, 41, 15
McGaugh, S. S. 1991, ApJ, 380, 140
Oke, J. B., et al. 1995, PASP, 107, 375
Pagel, B. E. J., Edmunds, M. G., Blackwell, D. E., Chun, M. S., & Smith, G. 1979, MNRAS, 189, 95
Petit, H., Hua, C. T., Bersier, D., & Courtès, G. 1996, A&A, 309, 446
Pettini, M., & Pagel, B. E. J. 2004, MNRAS, 348, L59
Pierce, M. J. 1986, AJ, 92, 285
Pilyugin, L. S. 2000, A&A, 362, 325
———. 2001, A&A, 369, 594
Pilyugin, L. S., Thuan, T. X., & Vílchez, J. M. 2003, A&A, 397, 487
Schaerer, D., & Vacca, W. D. 1998, ApJ, 497, 618
Scoville, N. Z., Polletta, M., Ewald, S., Stolovy, S. R., Thompson, R. I., & Rieke, M. 2001, AJ, 122, 3017
Shaw, R. A., & Dufour, R. J. 1995, PASP, 107, 896
Stasinska, G. 1978, A&A, 66, 257
———. 1990, A&AS, 83, 501
Stasinska, G., Schaerer, D., & Leitherer, C. 2001, A&A, 370, 1
Tayal, S. S., & Gupta, G. P. 1999, ApJ, 526, 544
Tilanus, R. P. J., & Allen, R. J. 1991, A&A, 244, 8
van Zee, L., Salzer, J. J., Haynes, M. P., O'Donoghue, A. A., & Balonek, T. J. 1998, AJ, 116, 2805
Vila-Costas, M. B., & Edmunds, M. G. 1992, MNRAS, 259, 121
Vílchez, J. M., & Pagel, B. E. J. 1988, MNRAS, 231, 257
Wilson, C. D. 1995, ApJ, 448, L97
Young, J. S., et al. 1995, ApJS, 98, 219
Zaritsky, D., Kennicutt, R. C., Jr., & Huchra, J. P. 1994, ApJ, 420, 87